A Detailed NMR-Based Model for CO on Pt Catalysts in an Electrochemical Environment: Shifts, Relaxation, Back-Bonding, and the Fermi-Level Local Density of States

YuYe Tong, Cynthia Rice, Andrzej Wieckowski,* and Eric Oldfield*

Contribution from the Department of Chemistry, University of Illinois at Urbana-Champaign, 600 South Mathews Avenue, Urbana, Illinois 61801

Received June 28, 1999. Revised Manuscript Received December 8, 1999

Abstract: ^{13}C NMR shift and spin−lattice relaxation measurements have been used to investigate ^{13}CO (ex MeOH) on fuel cell grade Pt electrodes (having average particle diameters of 2, 2.5, and 8.8 nm) in an electrochemical environment from 80 to 293 K at 8.47 and 14.1 T. The temperature dependence of the ^{13}C spin−lattice relaxation rate, $1/T_1$, shows a Korringa relationship which is independent of magnetic field, for all three samples. However, the peak positions and the corresponding T_1T values depend on particle size, with those of the 8.8 nm sample approaching values found for unsupported polycrystalline platinum black in an electrochemical environment (J. B. Day et al., *J. Am. Chem. Soc*. **1996**, *118*, 13046−13050). The ^{13}C T_1 is single exponential, independent of particle size and temperature, in contrast to previous results obtained on oxide-supported Pt−CO systems in a "dry" environment, in which relaxation was nonexponential at low temperatures, but exponential at high temperatures, suggesting strongly a quantum size effect in the dry systems at low *T*. A detailed two-band model is developed to analyze the partitioning of the Fermi level local density of states (E_f-LDOS) between the CO 5σ and 2π* orbitals and shows that the 2π*-like E_f-LDOS at ^{13}C is about 10 times larger than the 5σ-like E_f-LDOS. Smaller Pt particles have shorter ^{13}CO T_1 values and more downfield shifts, due to the increase in the 2π*-like E_f-LDOS. There is also a linear correlation between the value of the 2π*-like E_f-LDOS and the corresponding infrared stretching frequency, due to back-bonding. This indicates that the "Stark tuning" effect (the response of the vibrational stretch frequency to an applied field) is dominated by variations in the 2π*-like E_f-LDOS driven by the electrode potential, rather than a classical electrostatic effect. The two-band model developed here for ligand ^{13}C atoms complements that described previously for ^{195}Pt atoms in the metal electrode, and should be applicable to other nuclei and adsorbates as well, enabling Fermi level densities of states information to be obtained from both sides of the electrochemical interface, which can then be correlated with other spectroscopies (e.g., infrared) and chemical (e.g., catalytic activity) properties.

Introduction

The field of NMR-electrochemistry spectroscopy (NMRES) has witnessed considerable progress in recent years[1], and it is now technically possible to investigate in detail both adsorbates,[2−4] as well as Pt and Pt/Ru[5−8] metal surfaces, via solid-state NMR, in an electrochemical environment. This enables information about the electronic properties of electrocatalysts, alloying effects, electrode adsorption, surface diffusion of electrochemical adsorbates, and poisoning intermediates, to be deduced in an electrochemical environment which is close to real-world working conditions. This ability to access both physical and chemical information at both sides of the electrochemical interface also permits deeper insights to be obtained into structure and bonding at the solid−liquid interface, including the effects of electrode potential on the electronic properties of the chemisorption bond. In this paper, we report the first detailed ^{13}C NMR study of CO chemisorbed via methanol electrooxidation onto commercial carbon-black-supported fuel cell grade nanoscale platinum electrode surfaces, in an electrochemical environment. Experiments were carried out at two magnetic field strengths (8.47 and 14.1 T) over a wide temperature range (from 80 to 293 K), and on three electrocatalysts, having average particle sizes of 2.0, 2.5, and 8.8 nm. Our results suggest the presence of a metal−support interaction, which modifies the electronic properties of small platinum particles, and also strongly suggest that the electrode potential alters the electronic properties of chemisorbed CO. We also compare and contrast the ^{13}C spin−lattice relaxation behavior seen between carbon- and oxide-supported Pt−CO systems, and develop a phenomenological two-band model for the ^{13}C NMR observables of chemisorbed CO in the metallic state. Using this theoretical

(1) Tong, Y. Y.; Oldfield, E.; Wieckowski, A. *Anal. Chem.* **1998**, *70*, 518A-527A.
(2) Day, J. B.; Vuissoz, P.-A.; Oldfield, E.; Wieckowski, A.; Ansermet, J.-P. *J. Am. Chem. Soc.* **1996**, *118*, 13046−13050.
(3) Wu, J. J.; Day, J. B.; Franaszczuk, K.; Montez, B.; Oldfield, E.; Wieckowski, A.; Vuissoz, P.-A.; Ansermet, J.-P. *J. Chem. Soc., Faraday Trans.* **1997**, *93*, 1017−1026.
(4) Yahnke, M. S.; Rush, B. M.; Reimer, J. A.; Cairns, E. J. *J. Am. Chem. Soc.* **1996**, *118*, 12250−12251.
(5) Tong, Y. Y.; Belrose, C.; Wieckowski, A.; Oldfield, E. *J. Am. Chem. Soc.* **1997**, *119*, 11709−11710.
(6) Tong, Y. Y.; Rice, C.; Godbout, N.; Wieckowski, A.; Oldfield, E. *J. Am. Chem. Soc.* **1999**, *121*, 2996−3003.
(7) Rice, C.; Tong, Y. Y.; Oldfield, E.; Wieckowski, A. *Electrochim. Acta* **1998**, *43*, 2825−2830.
(8) Tong, Y. Y.; Rice, C.; Wieckowski, A.; Oldfield, E., unpublished results.

10.1021/ja9922274 CCC: $19.00
Published on Web 01/28/2000

model, we deduce values for the Fermi level local density of states (E_f-LDOS) at ^{13}C, and obtain for the first time a partitioning of the E_f-LDOS between CO's 5s and $2\pi^*$ orbitals. This provides new insights into the electronic origins of the physical as well as the chemical properties of chemisorbed CO, which we will use elsewhere to investigate the effects of Ru-alloying in overcoming CO poisoning in Pt fuel cell catalysts.[8]

Experimental Section

The electrode materials used were carbon-black (XC-72)-supported commercial fuel cell grade nanoscale platinum electrocatalysts (E-TEK Inc., Natrick, MA). The average particle sizes (provided by E-TEK) were 2.0, 2.5, and 8.8 nm, as determined by X-ray diffraction. The size distribution was not specified. The NMR samples were prepared in a conventional three-electrode cell, containing a platinum gauze counter electrode, a 1 M NaCl Ag/AgCl reference electrode, and a working electrode consisting of supported platinum catalyst particles (approximately 500 mg) contained in a platinum boat. The cell potential was controlled by a PGP201 potentiostat/galvanostat manufactured by Radiometer (Villeurbanne, France). The electrolyte used was 0.5 M H_2SO_4 and was prepared from concentrated analytical grade sulfuric acid from Mallinckrodt Baker Inc. (Paris, Kentucky), using Milli-pore (Millipore, Corp., Bedford, MA) water. Chemisorbed ^{13}CO was produced from the electrochemical decomposition of 99% ^{13}C-labeled methanol (Cambridge Isotopes Laboratories, Cambridge, MA) in 0.5 M H_2SO_4 on pre-cleaned[7] platinum surfaces at a potential of 0 mV with respect to a Ag/AgCl (1.0 M) reference electrode. After adsorption, the electrode material (together with supporting electrolyte, and under oxygen-free N_2 or Ar) was transferred into a 10 mm diameter × 25 mm length tube, and flame-sealed under vacuum. A small portion of sample was left in the cell and was used to determine the CO coverage.

Cyclic voltammetry (CV) was performed in the same electrochemical cell as mentioned above, using from 50 to 380 mg of platinum particles (to reduce the I-loading of the cell). The particles were loosely arranged on top of one another in the Pt boat, allowing contact between each Pt particle and the solvent. The CV current increase was proportional to the quantity of sample added to the Pt boat. This proportionality suggests that the setup used permits each particle to contribute equally to the overall current. The ^{195}Pt NMR spectra confirm that the surfaces of the electrocatalysts are clean.[1,6] Initially, the cell potential was held at 250 mV for 1 to 2 h, until the current decreased to insignificant levels, and then the cell potential was swept at a rate of 20 mV/min in the potential range from −270 to 1050 mV.

All NMR measurement were carried out on "home-built" NMR spectrometers equipped with 3.5 in. bore 8.45 and 14.1 T superconducting magnets (Oxford Instruments, Osney Mead, Oxford, UK), Tecmag (Houston, TX) Aries data acquisition systems, and (at 8.47 T) using an Oxford Instruments CF-1200 cryostat. A Hahn spin−echo pulse sequence ($\pi/2 - \tau_0 - \pi - \tau_0 -$ acquire) with 16-step phase cycling to eliminate ringdown, was used for data acquisition. Chemical (or frequency) shifts for ^{13}C are given in ppm from tetramethylsilane (TMS), using the International Union of Pure and Applied Chemistry δ-scale convention (high-frequency, low-field, paramagnetic or deshielded values are positive), and were measured experimentally with respect to an external standard of CS_2 ($\delta = 192.8$ ppm from TMS). All spin−lattice relaxation times were measured by monitoring amplitude variation at maxima of ^{13}CO NMR peaks, using an inversion−recovery method, which consisted of a preparative composite π pulse,[9] $(\pi/2)_x$-$(3\pi/2)_y(\pi/2)_x$, followed by the aforementioned Hahn-echo acquisition sequence, with τ_0 set to either 30 μs or 35 μs. If not specified, the $\pi/2$ pulse length was typically between 5 and 8 μs, depending on experimental details.

Results

We show in Figure 1 the ^{13}C NMR spectra of CO chemisorbed onto carbon-supported commercial fuel cell grade Pt electrocatalysts having different particle sizes, together with (insets) their corresponding cyclic voltammograms. Spectra were recorded at 14.1 T and at 293 K. The relatively long 90° pulse width in such conducting samples did not permit the whole spectral region to be uniformly irradiated. We therefore used a spin−echo mapping technique[10] to reconstruct the entire spectrum from several sub-spectra. The frequency increment used to record each sub-spectrum was ∼15 kHz. The number of scans (repetition time) for each subspectrum were: 4800 (1.5 s), 12000 (1 s), 24000 (1s) for spectra A, B, and C, respectively. The line broadening used was 1 kHz. The peak at 170 ppm comes from the graphitized carbon support, which is distinguishable from chemisorbed CO by its spin−lattice relaxation behavior. We show in Table 1 the data for CO coverage, ^{13}C peak position and the line width obtained by using a Gaussian/Lorentzian fit to the two peaks of the spectrum. As can be seen from Table 1 and Figure 1, the ^{13}CO NMR results are particle size dependent. In particular, the peak broadens as the particle size decreases, and this broadening appears to reflect the diversity of surface sites available for Pt−CO bonding, rather than any intrinsic spin−spin relaxation effect, as we discuss below in detail.

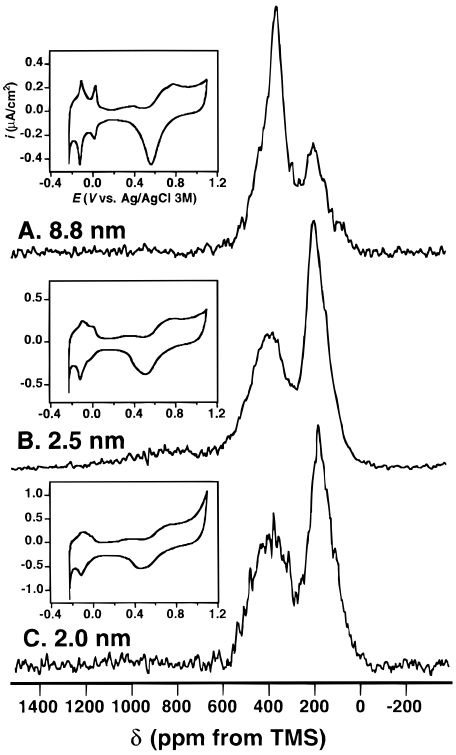

Figure 1. 14.1 T ^{13}C NMR spectra of chemisorbed CO on: (A) 8.8 nm, (B) 2.5 nm, and (C) 2.0 nm particle size Pt−carbon (E-TEK, Inc.) samples. Insets are the corresponding electrochemical cyclic voltammograms.

The CVs in the insets of Figure 1 show the macroscopic current-vs-potential relationships arising from the characteristic charge-transfer behavior taking place at the electrochemical interface when cyclically sweeping the applied potential within a given range. In the case of platinum, adsorption and desorption of hydrogen occur in the negative potential region (<50 mV), while oxygen adsorption takes place in the positive potential region (>450 mV), and the surface-oxide reduction peak appears at ∼450 mV when the potential is swept in the negative direction. The well-resolved peaks in the hydrogen evolution region for the largest particles (8.8 nm) are characteristic features

(9) Freeman, R.; Kempsell, S. P.; Levitt, M. H. *J. Magn. Reson.* **1980**, *38*, 453−479.

(10) Tong, Y. Y. *J. Magn. Reson. A* **1996**, *119*, 22−28.

Table 1. ^{13}C NMR Data for CO ex. MeOH on Carbon-Supported Pt Nanoparticles

size (nm)	coverage (%)	peak shift (ppm)	fwhm (ppm)	T_1T (s·K)[a]	B	$(1/T_1)_{orb+dip}$ (s^{-1})
8.8[b]	65 ± 4	351 ± 1	102 ± 2	68 ± 2	4.9 ± 0.6[c]	0.96 ± 0.02[c]
2.5[b]	56 ± 3	386 ± 2	174 ± 5	59 ± 3	3.6 ± 0.1[c]	1.07 ± 0.01[c]
2.0[b]	64 ± 4	376 ± 5	245 ± 10	55 ± 4	7.7 ± 2.2[c]	1.25 ± 0.04[c]
					4.5 ± 0.6[d]	2.22 ± 0.09[d]
2.5[e]	35 ± 2	390 ± 2	177 ± 7	51± 5	- - - -	- - - -

[a] Measured at the peak positions. [b] Electro-oxidation of MeOH carried out at 0 mV with respect to a Ag/AgCl (1 M NaCl) reference electrode. [c] From data obtained at 80 K. [d] From data obtained at 150 K. [e] Electro-oxidation of MeOH carried out at −150 mV with respect to a Ag/AgCl (1 M NaCl) reference electrode.

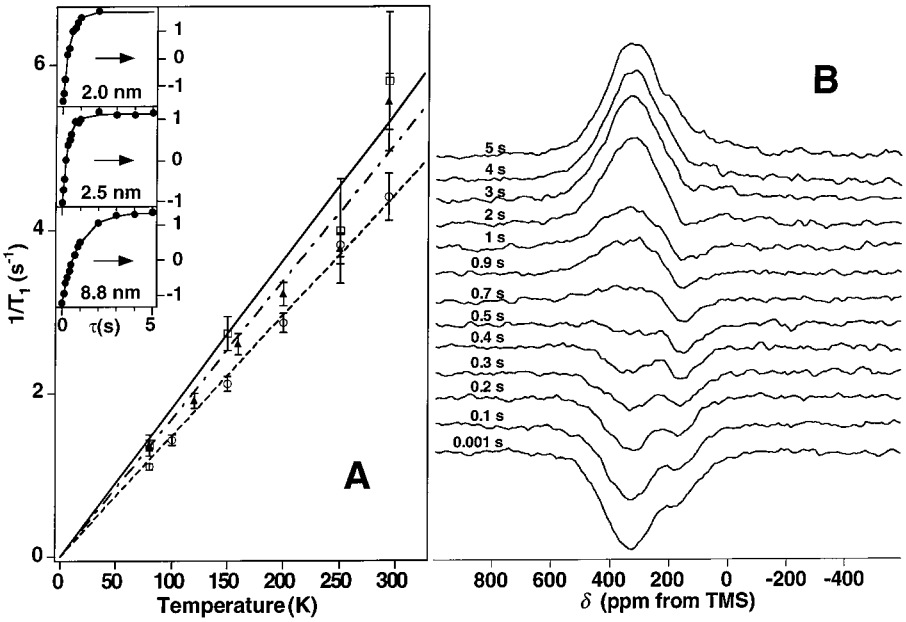

Figure 2. Temperature dependence of the ^{13}C NMR spin−lattice relaxation rate at 8.45 T for chemisorbed CO, measured at the ^{13}CO peak maxima in Figure 1. (A) open circles, 8.8 nm; filled triangles, 2.5 nm; and open squares, 2.0 nm particle size samples. Note that the points at 293 K were taken at a magnetic field of 14.1 T, while all other points were obtained at 8.5 T. The straight (dash for 8.8 nm, dash−dot for 2.5 nm, and solid for 2.0 nm samples) lines, which pass through the origin, are the fits to the data, indicating Korringa relationships, and give the T_1T values shown in Table 1. The insets are typical inversion−recovery spin−lattice relaxation curves, with solid lines representing single-exponential fits. In B are a set of inversion−recovery T_1 spectra taken on the 8.8 nm sample at 80 K, which gave the relaxation curve shown in the corresponding inset. The data acquisition parameters were: $\pi/2$ pulse length = 6 μs, composite 180° pulse, repetition time = 5 s, and line broadening = 1500 Hz. The list of times shown in Figure 2B were the interval values between the preparative inversion and the acquisition pulses.

of randomly oriented single crystal surfaces, i.e., the signature of relatively well-defined, large, smooth surfaces. However, these features gradually disappear as the particle sizes decrease, and for the sample having an average particle size of 2.0 nm, these features are no longer visible, inset in Figure 1C, due to the disperse nature of the Pt/Pt−H environments.

In Figure 2A, we show the temperature dependence of the spin−lattice relaxation rate, $1/T_1$, measured at the maxima of the ^{13}CO NMR peaks using the inversion−recovery method, between 80 and 293 K, for the 8.8, 2.5, and 2.0 nm samples. Although some data points do overlap (for example those at 250 K), the different data sets still obey the Korringa relationship: T_1T = constant, as evidenced by the straight lines obtained for the $1/T_1$ vs T correlations, Figure 2A. These results indicate that relaxation is dominated by conduction electron spin fluctuations at the respective ^{13}C nuclei. The values for T_1T, obtained from a linear fit to the data, are shown in Table 1. Note that the data points at 293 K (Figure 2) were taken at a magnetic field of 14.1 T, while all other points were obtained at 8.5 T. The magnetic field independence of T_1T (Table 1 and Figure 2) also points to the presence of conduction electron spin fluctuations at the ^{13}C sites, since Korringa relaxation is field-independent. Without exception, all relaxation curves are single exponential, even down to 80 K, and typical relaxation recovery curves are shown in the insets, with the solid lines representing single-exponential fits. In Figure 2B, we also show a representative inversion−recovery T_1 data set from which the relaxation curve shown in the inset, Figure 2A, was obtained. For this set of experiments, carried out at 80 K, the $\pi/2$ pulse length was 6 μs, τ_0 set to 35 μs, the number of scans and repetition time were 640 and 5 s, respectively, and a 1.5 kHz line broadening, due to exponential multiplication, was used. Note that the observation of single exponential relaxation behavior at a given shift is in sharp contrast to results obtained previously in "dry" (oxide-supported) cases,[11] where relaxation of CO was universally found to be nonexponential at low temperatures, but single exponential above room temperature.

We show in Figure 3 the ^{13}C NMR spectrum of CO adsorbed onto the same electrocatalyst as that of Figure 1B (a 2.5 nm material) but having a different coverage. For the spectrum shown here, catalytic decomposition of methanol was carried out at a potential of −150 mV, instead of the 0 mV used for all other samples. The CO coverage, θ, determined by CV, was 0.35, which should be compared with θ = 0.56 for the sample shown in Figure 1B. The room temperature (293 K) spin−lattice relaxation time for the θ = 0.35 sample, measured at ∼390

(11) Dean, E. J. Ph.D, University of Illinois at Urbana-Champaign, 1997.

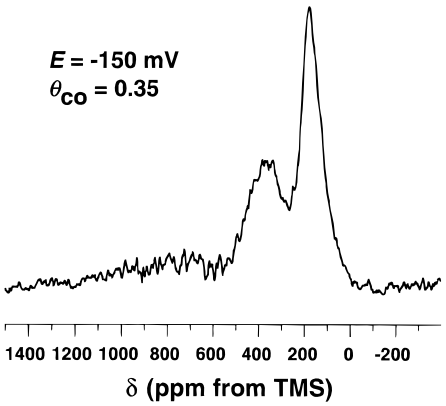

Figure 3. 14.1 T ^{13}C NMR spectrum of CO on 2.5 nm Pt−carbon sample with a CO coverage of 0.35. Note that the electrooxidation of methanol was carried out at a potential of −150 mV with respect to Ag/AgCl (1 M, NaCl) reference electrode. This should be compared to Figure 1B since both samples were from the same batch but with different CO coverages, produced through electrooxidation of methanol at different potentials.

ppm, was 175 ± 17 ms, giving a $T_1T = 51 \pm 5$ s·K, which is smaller than that of the high coverage sample, $T_1T = 59 \pm 3$ s·K (Table 1).

Finally, we show in Figure 4A strong evidence for a T_1 anisotropy across the ^{13}CO NMR spectra. This spectrum was obtained at 80 K on the same sample whose spectrum is shown in Figure 2B, and represents a partially relaxed Fourier transform spectrum at $\tau = 500$ ms (the τ-values representing the time between the composite π pulse inversion and the Hahn-echo acquisition sequence). To obtained a sufficient signal/noise ratio, however, the number of scans was 8848, much larger than 640 used for the spectrum shown in Figure 2B. As can be seen from Figure 4A, signals above/below ∼356 ppm show positive/negative amplitudes at this particular relaxation interval, indicating that nuclei resonating at higher frequencies (low-field) relax faster. In Figure 4B, we show a typical variation of the spin−lattice relaxation rate across a spectrum, measured at 80 K on the 2.5 nm sample by monitoring the recovery of the signal at a given shift position, which was incremented. All of the relaxation curves obtained were again single exponential, reflecting the inhomogeneous nature of the resonance. That is, the nuclear spin isochromat at a given resonance frequency relaxes independently, dictated only by its local electronic environment. The solid line in the figure is the fit to the equation:

$$1/T_1 = (\delta - \delta_{\mathrm{orb}})^2 T/SB + (1/T_1)_{\mathrm{orb+dip}} \qquad (1)$$

where the Korringa ratio, B, and $(1/T_1)_{\mathrm{orb+dip}}$ are fitting parameters; T is the absolute temperature; $S = (\gamma_e/\gamma_n)^2(\hbar/4\pi k)$ is the Korringa constant (4.16×10^{-6} s·K for ^{13}C); and δ_{orb} is the orbital shift, taken to be 160 ppm, based on previous density functional theory calculations and model compound results.[6] The first term in eq 1 is the pure Korringa term and arises from the hyperfine interactions which are also responsible for the pure Knight shift; the second term accounts for spin−lattice relaxation contributions from both orbital and dipolar interactions. The fitted results of Figure 4A, together with those of the other samples, are collected in Table 1. Note that the more the constant B deviates from unity, the stronger the electronic many-body effects are. For example, the experimental B value for bulk platinum is ∼6. After Obata,[12] we have for a $2\pi^*$ orbital, the following equation for the orbital and dipolar

(12) Obata, Y. *J. Phys. Soc. Jpn.* **1963**, *18*, 1020−1024.

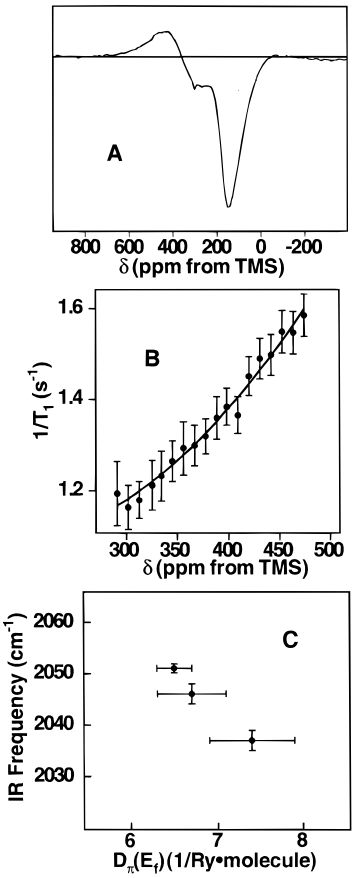

Figure 4. (A) 8.5 T partially relaxed ^{13}CO spectrum, recorded on 8.8 nm sample at 80 K. The time interval between inversion and acquisition pulses was 500 ms; the $\pi/2$ pulse length was 7 μs, repetition time 4.5 s, number of scans 8848, and line broadening 1000 Hz. The node point separating positive and negative signals is at ca. 356 ppm. (B) 8.5 T ^{13}C NMR spin−lattice relaxation rates across a spectrum, measured at 80 K on a 2.5 nm particle size sample. The solid line is a fit to eq 1. The fitted results, together with those of other samples, are given in Table 1. (C) Correlation between CO IR stretching frequencies for 8, 2.5, and 2.0 nm samples and the corresponding $D_\pi(E_f)$'s. The data can be fitted by a straight line having an intercept of 2147 ± 30 cm^{-1}, a slope of −15 ± 2 cm^{-1}/(Ry·atom)$^{-1}$, and a $R^2 = 0.99$. The error bars in $D_\pi(E_f)$ are the uncertainties propagated from those in T_1T.

contributions:

$$(1/T_1)_{\mathrm{orb+dip}} = (13/5)(T/S)(\mu_B H_{\mathrm{orb},\pi} D_\pi(E_f))^2 \qquad (2)$$

where μ_B is the Bohr magneton, $H_{\mathrm{orb},\pi}$ is the π-orbital hyperfine field, and $D_\pi(E_f)$ is the Fermi level local density of states of the $2\pi^*$ orbital.

Since our following discussions are largely based on the NMR results, particularly the T_1's, measured at the peak maximum, while the T_1 varies across the spectrum, a legitimate concern is how meaningful such an approach is. Strictly speaking, the mean value of the spin−lattice relaxation time across the spectrum, $T_1^{\mathrm{av}} = \sum a(\nu)T_1(\nu)/\sum a(\nu)$—where a is the signal amplitude at frequency ν, should be used for meaningful comparison. However, in the cases studied here, the T_1 measured at the peak position is actually a very good approximation of T_1^{av}, because: (1) all ^{13}CO spectra obtained are almost symmetric and (2) the T_1 variation across the spectrum is also quite symmetric with respect to the value measured at the peak maximum, Figure 4B. Thus, the T_1's measured at the peak positions are valid values for comparison, and even T_1 may vary across the spectrum for a given sample. With this background information,

we now consider the origins of the frequency-dependent relaxation and frequency shifts seen in different catalyst samples and then compare these results with those obtained from infrared spectroscopy.

Discussion

The observation of Korringa relaxation behavior, as shown in Figure 2, demonstrates that CO adsorbed onto conductive-material-supported small platinum particle surfaces is in a metallic state. Since the Korringa relationship has previously been found to apply to CO adsorbed onto polycrystalline platinum black (8.0 nm) in the same electrochemical environment,[2] as well as on oxide-supported small platinum clusters,[13] such a general statement seems unsurprising. However, a detailed inspection of the results, Table 1, reveals three interesting new observations, which as discussed below in detail have led us to develop a new, detailed, two-band model for ^{13}C relaxation (and shifts) in such catalyst systems, which may, we believe, find widespread use in investigating these and related materials.

The first new observation is that there appears to exist a strong metal−support interaction which alters the electronic properties of the Pt particles. For example, the 8.8 nm sample has a ^{13}C shift of 351 ppm and a $T_1T = 68 \pm 2$ s·K, close to the values found previously for unsupported polycrystalline platinum black[2]: $\delta = 330$ ppm and $T_1T = 78 \pm 3$ s·K, while for the smaller samples (2.0 and 2.5 nm), an enhancement of the metallic state is observed. That is to say, the ^{13}C shift is even more downfield, at ∼380 ppm from TMS, and is accompanied by a more effective spin−lattice relaxation, that is, a smaller T_1T, around 57 s·K versus 68 ± 2 s·K for the large particles. The presence of the electrochemical solid/liquid interface per se seems unlikely to be the primary source for such an enhancement, since all of the experimental conditions and procedures were the same for the three samples. We believe, therefore, that this enhancement arises primarily from a stronger interaction between the platinum particle and the carbon support. There are two major reasons for this belief: First, our ^{195}Pt NMR study of the same electrocatalyst (but without CO adsorption)[6] suggested that a small portion of surface platinum atoms behave differently from the rest, due most probably to a direct interaction with the (conducting) carbon support. Second, it is reasonable to assume that the larger the particle is, the less the support influence will be "felt" by the particle as a whole. This is indeed what is observed: the larger the Pt particle, the closer the properties are to those of unsupported platinum black.

The second new observation is that the spin−lattice relaxation of adsorbed CO, measured at any given shift, is single exponential, even down to a temperature as low as 80 K and with samples as small as 2 nm. Similar single exponential relaxation behavior has been observed previously for unsupported polycrystalline platinum black, also in an electrochemical environment.[2] Such single-exponential relaxation behavior for ^{13}CO adsorbed on carbon-supported small platinum particles is somewhat surprising, since it is in sharp contrast to results obtained previously for CO adsorbed onto oxide (Al_2O_3)-supported platinum particles having similar sizes in the "dry" phase,[11] where the ^{13}C relaxation was nonexponential below room temperature, but converged to a single exponential above 333 K, having a $T_1T = 46$ s·K.[14] Since the presence of heterogeneity at the metal surface does not produce any observable nonexponential relaxation in the carbon-supported particles, the nonexponential relaxation behavior seen in the oxide samples at low temperatures most likely arises from the presence of the so-called quantum size effect.[15] That is, there are substantially fewer electrons in the small Pt particles, as opposed to those in the bulk, which does not enable a bulklike Pauli paramagnetism to be seen by the adsorbate. Since all carbon-supported Pt-^{13}CO relaxation curves were single exponential, even though surface heterogeneity makes a major contribution to the spectral line width, it is unlikely that surface heterogeneity would be a major reason for the nonexponential relaxation observed in oxide-supported Pt−CO systems, at low temperatures.

The third new observation is that the ^{13}CO NMR spectrum broadens as the particle size decreases, consistent with the electrochemical data, which indicates an increase in surface heterogeneity, Figure 1. This suggests that the observed ^{13}C line breadths reflect the heterogeneity of the surfaces onto which the CO is adsorbed, that is, the whole ^{13}CO NMR spectrum is composed of many, much narrower lines, each having a slightly different shift. A conclusion similar to this has been reached previously via "magic-angle" sample spinning studies of oxide supported Pt−CO and Pd−CO systems.[16] In addition, strong evidence for this heterogeneity comes from the variation in spin−lattice relaxation rate seen across the spectrum, as shown for example in Figure 4A, B. A steady increase in the relaxation rate is observed as the ^{13}C shift becomes more positive (low-field), indicating that different peak locations correspond to different Pt−CO bonding situations, rather than to an (anisotropic) orientation dependence, such as found, for example, with the chemical shift anisotropy. This is again in agreement with the results of previous ^{13}C NMR studies of oxide supported Pt−CO and Pd−CO systems.[16,17]

Since we failed to observe the CO coverage dependence of ^{13}C NMR reported in ref 4 (Figure 3 vs Figure 1B), and since our recent in situ infrared results on these same systems have not revealed any significant amount of bridge-bonded species,[18] it is reasonable to assume that the variation in $1/T_1$ across the spectra arise only from the site-to-site variations in the Knight shift of the terminal CO on the metal surface. We can therefore fit the data in Figure 4A by using eq 1, with two parameters: B, accounting for electronic many-body effects, that is, the exchange/correlation interactions; and $(1/T_1)_{orb-dip}$ for the orbital and dipolar contributions. Final fitted results are shown for four data sets in Table 1. The significant deviation from unity for B strongly suggests that it is necessary to take into account in some way these exchange/correlation interactions, when analyzing the ^{13}C NMR data, as described below.

A Two-Band Model for ^{13}C NMR. By analogy with the two-band model previously developed for analyzing ^{195}Pt NMR data,[6,19,20] in which electronic many-body effects were taken into account through the Stoner enhancement factor in the Knight shift and the Shaw−Warren de-enhancement factor in the spin−lattice relaxation rate (vide infra), we can write down

(13) Slichter, C. P. *Annu. Rev. Phys. Chem.* **1986**, *37*, 25−51.
(14) Rudaz, S. L.; Ansermet, J.-P.; Wang, P.-K.; Slichter, C. P. *Phys. Rev. Lett.* **1985**, *54*, 71−74.
(15) Halperin, W. P. *Rev. Mod. Phys.* **1986**, *58*, 533−606.
(16) Zilm, K. W.; Bonneviot, L.; Hamilton, D. M.; Webb, G. G.; Haller, G. L. *J. Phys. Chem.* **1990**, *94*, 1463−1472.
(17) Zilm, K. W.; Bonneviot, L.; Haller, G. L.; Han, O. H.; Kermarec, M. *J. Phys. Chem.* **1990**, *94*, 9495−8498.
(18) Rice, C.; Tong, Y. Y.; Oldfield, E.; Wieckowski, A.; Hahn, F.; Gloaguen, F.; Léger, J.-M.; Lamey, C., unpublished results.
(19) Bucher, J. P.; van der Klink, J. J.; *Phys. Rev. B.* **1988**, *38*, 11038−11047.
(20) van der Klink, J. J.*; The Surface of Supported Metal Catalysts Probed by NMR*, In *Advances in Catalysis.*; Academic Press: New York, 2000; Vol. 44, pp 1−117.

the following equations for the ^{13}C Knight shifts and relaxation rates:

$$K = K_\sigma + K_\pi + K_{\text{orb}} = \mu_B D_\sigma(E_f) H_{\text{hf},\sigma}/(1-\alpha_\sigma) + \mu_B D_\pi(E_f) H_{\text{hf},\pi}/(1-\alpha_\pi) + K_{orb} \quad (3)$$

$$S(T_1T)^{-1} = k(\alpha_\sigma)K_\sigma^{\,2} + k(\alpha_\pi)K_\pi^{\,2}/2 + S(T_1T)^{-1}_{\text{orb+dip}} = k(\alpha_\sigma)K_\sigma^{\,2} + k(\alpha_\pi)K_\pi^{\,2}/2 + (13/5)(\mu_B H_{\text{hf,orb}} D_\pi(E_f))^2 \quad (4)$$

where $D_\sigma(E_f)$ and $D_\pi(E_f)$ are the σ-like and π-like densities of states at the Fermi level; $H_{\text{hf,l}}$, with l = σ, π, and orb, stand for 5σ-band, 2π*-band, and orbital contributions. No inter-band interactions are taken into account, but the separate σ-like and π-like Stoner factors are introduced as:

$$\alpha_l = I_l D_l(E_f) \quad \text{with} \quad l = \sigma, \pi \quad (5)$$

where I_σ and I_π are exchange integrals. The relationship between the Stoner and Korringa de-enhancement factors, $k(\alpha)$, are assumed to be given by the Shaw−Warren relationship,[21] for both σ-like and π-like electrons.

Now, to deduce the $D_\sigma(E_f)$ and $D_\pi(E_f)$ from eqs 3 and 4, we need to know the orbital shift, K_{orb}, the hyperfine fields $H_{\text{hf},\sigma}$, $H_{\text{hf},\pi}$, and $H_{\text{hf,orb}}$, and the exchange integrals, I_σ and I_π. For carbon in CO, $H_{\text{hf},\sigma}$ and $H_{\text{hf},\pi}$ have been determined experimentally from the electron spin resonance of CO^+ and CO^-, and have values of 363 and 17 kG, respectively.[22,23] For on-top bonding of CO on a platinum surface, K_{orb} has been calculated recently via density functional theory[6] and has a value of 160 ppm with respect to TMS. No data on I_σ and I_π are available for CO; however, as an approximation, we can set I_σ = the I value (0.086 Ry)[24] for Li, an s-band metal, and I_π = the I value (0.078 Ry)[24] for Be, a p-band metal. Since both are close to carbon in the Periodic Table, and I changes only slowly for elements within the same row,[24] we believe that these are reasonable approximations for ^{13}C in a metallic environment.

With all these values, we are now ready to estimate the value of $H_{\text{hf,orb}}$. First, eqs 3, 4, and 5 can be rearranged as follows:

$$K - K_{\text{orb}} = \mu_B D_\sigma(E_f) H_{\text{hf},\sigma}/(1 - I_\sigma D_\sigma(E_f)) + \mu_B D_\pi(E_f) H_{\text{hf},\pi}/(1 - I_\pi D_\pi(E_f)) \quad (6)$$

$$S(T_1T)^{-1} - S(T_1T)^{-1}_{\text{orb+dip}} = k(I_\sigma D_\sigma(E_f))K_\sigma^{\,2} + k(I_\pi D_\pi(E_f))K_\pi^{\,2}/2 \quad (7)$$

Since K_{orb} = 160 ppm,[6] and K, $S(T_1T)^{-1}$, and $S(T_1T)^{-1}_{\text{orb+dip}}$ can be obtained from the values listed in Table 1, eqs 6 and 7 are two simultaneous equations for the unknowns: $D_\sigma(E_f)$ and $D_\pi(E_f)$, which can be deduced for each of the three samples investigated. Then, using $D_\pi(E_f)$ and the corresponding value for $(1/T_1)_{\text{orb+dip}}$ in Table 1, we can evaluate $H_{\text{hf,orb}}$ by using eq 2. We find $H_{\text{hf,orb}}$ = 49, 52, 48, and 50 kG from the data sets for the 2.0 (2 sets), 2.5, and 8.8 nm samples, which gives $H_{\text{hf,orb}}$ = 50 kG, on average. Note that no sign has been experimentally determined for $H_{\text{hf},\pi}$. However, a positive sign has previously been reported for core-polarization produced by 2p or 3p electrons,[25] and in fact only this positive sign gives physically meaningful results when solving eqs 6 and 7 (i.e., with Stoner enhancement factors between 0 and 1).

Table 2. Parameters Used for E_f-LDOS Analysis.

K_{orb} (ppm)	I_σ (Ry)	I_π (Ry)	$H_{\text{hf},\sigma}$ (kG)	$H_{\text{hf},\pi}$ (kG)	$H_{\text{hf,orb}}$ (kG)
160[a]	0.086[b]	0.078[b]	363[c]	17[d]	50[e]

[a] Reference 6. [b] Reference 24. [c] Reference 22. [d] Reference 23. [e] Determined in this work.

Table 3. E_f-LDOS's for Chemisorbed CO

size (nm)	$D_\sigma(E_f)$[a] (Ry·molecule)$^{-1}$	$D_\pi(E_f)$[a] (Ry·molecule)$^{-1}$	$D_{\text{total}}(E_f)$ (Ry·molecule)$^{-1}$
8.8[b]	0.6 ± 0.1	6.5 ± 0.2	7.1
2.5[b]	0.7 ± 0.2	6.7 ± 0.3	7.4
2.0[b]	0.6 ± 0.2	7.4 ± 0.4	8.0
2.5[c]	0.6 ± 0.2	7.6 ± 0.5	8.2

[a] Deduced by using eqs 3 and 4 and the K and T_1T data in Table 1. The errors in E_f-*LDOS* stand only for the uncertainty propagated from those in T_1T. [b] Electro-oxidation of MeOH carried out at 0 mV with respect to a Ag/AgCl (1 M NaCl) reference electrode. [c] Electro-oxidation of MeOH carried out at −150 mV with respect to a Ag/AgCl (1 M NaCl) reference electrode.

Using the set of parameters given in Table 2, which include the *average* value for $H_{\text{hf,orb}}$ (which is expected to be more accurate than any individual single-point determination), eqs 3 and 4 can now be solved to deduce precise values for $D_\sigma(E_f)$ and $D_\pi(E_f)$ of chemisorbed CO when the values of K and T_1T are known. We therefore recalculated the values of $D_\sigma(E_f)$ and $D_\pi(E_f)$ using the values of K and T_1T in Table 1, and show these results in Table 3.

Note that when the orbital-plus-dipolar contribution to the total spin−lattice relaxation can be determined, eqs 6 and 7 are as good as eqs 3 and 4 for deducing $D_\sigma(E_f)$ and $D_\pi(E_f)$. However, it is usually rather difficult, if not impossible, to separate experimentally the orbital-plus-dipolar contribution from the total spin−lattice relaxation rate; eqs 3 and 4, therefore, provide a more general approach to the problem provided $H_{\text{hf,orb}}$ can be determined, as we have done above.

The results shown in Table 3 indicate that the contribution from π-like electrons to the ^{13}C NMR observables is dominant in all cases. The major part of the total E_f-LDOS at ^{13}C is from the π-like electrons, with $D_\pi(E_f)$ being about 10 times larger than $D_\sigma(E_f)$. The contribution to the spin−lattice relaxation rate, $1/T_1$, is dominated by orbital and dipolar interactions, consistent with the dominance of π-like electrons at the Fermi level. However, since NMR only measures the electron density at a given energy level, that is, the Fermi level, it does not provide complete information about the total electron densities for forward- and back-donation, which are the integrals of the LDOS from the bottom of the conduction band to the Fermi level. Nevertheless, as can be seen in Table 3, the change in the total E_f-LDOS over different samples is mainly due to the change in $D_\pi(E_f)$, which suggests that the changes in chemical properties of adsorbed CO are mainly determined by variations in back-bonding.

Theoretically, it has been shown previously[26] for CO adsorption on Pt(111), Ni(111), and Pd(111) surfaces, that 5σ forward-donation does not change significantly when CO moves from μ_1-, to μ_2-, and to μ_3-bonding positions, while 2π* back-donation increases significantly. This strongly suggests that the observed

(21) Shaw, R. W., Jr.; Warren, W. W., Jr. *Phys. Rev. B* **1971**, *3*, 1562−1568.
(22) Vedrine, J. C.; Naccache, C. *Chem. Phys. Lett.* **1973**, *18*, 93−95.
(23) Lunsford, J. H.; Jayne, J. P. *J. Chem. Phys.* **1966**, *44*, 1492−1502.
(24) Janak, J. F. *Phys. Rev. B* **1977**, *16*, 255−262.
(25) Carter, G. C.; Bennett, L. G.; Kahan, D. J. *Metallic Shifts*; Pergamon: New York, 1977; Vol. 20, Part I.
(26) Wong, Y.-T.; Hoffmann, R. *J. Phys. Chem.* **1991**, *95*, 859−867.

variation in stretching frequency with bonding geometry, decreasing from μ_1-, to μ_2-, and to μ_3-positions, is due to differences in back-donation. If it is indeed the case that the changes in $D_\pi(E_f)$ are an indication of the variations in back-donation, one would expect that the infrared vibrational stretch frequency of adsobed CO would change accordingly. Using recently obtained IR results from Lamy et al.[18] on the same sample batches as those we have investigated here, a clear correlation between the E_f-LDOS results shown in Table 3 and the corresponding IR stretch frequencies can be seen. The IR results are: $\nu_{CO} = 2051$ cm^{-1} (8.8 nm), 2046 cm^{-1} (2.5 nm), 2037 cm^{-1} (2.0 nm), and when plotted against the corresponding values for $D_\pi(E_f)$ (Table 3), we obtain a result shown in Figure 4C, which can be fitted by a straight line with an intercept of 2147 ± 30 cm^{-1} (close to the value expected for free CO,[27] $\nu = 2143$ cm^{-1}) and a slope of -15 ± 2 cm^{-1}/(Ry·molecule)$^{-1}$, which is consistent with previous results.[28]

The linear correlation found above also indicates a monotonic relationship between the $D_\pi(E_f)$, that is, the electron density at the Fermi level, and the total electron density of back-donation, that is, the integral of the LDOS from the bottom of $2\pi^*$ band to the Fermi level. This implies that the Fermi level cuts the tail of the $2\pi^*$ band as it is rising, that is, an increase in $D_\pi(E_f)$ indicates an enhancement in back-donation. This is consistent with the results of Masel and co-workers who found, using ultraviolet/high-resolution electron energy loss spectroscopy, that the CO's $2\pi^*$ level is lowered 0.6 eV upon adsorbed onto Pt (110),[29] and with the results of extended Hückel theory calculation[30]. It is also of interest to point out that the theoretical study predicts that the $D_\pi(E_f)$ dominates the total E_f-LDOS,[30] as we have found here.

Another important observation we can make is related to the electrode potential effects on the E_f-LDOS of adsorbed CO. For CO electro-chemisorbed onto the 2.5 nm sample at -150 mV, instead of at 0 mV (vs Ag/AgCl (1M, NaCl)), we found an increase of 0.9 (Ry·molecule)$^{-1}$ in $D_\pi(E_f)$ with no appreciable change in $D_\sigma(E_f)$, Table 3. Using the linear correlation found above, and neglecting the possible effect due to the change in $D_\sigma(E_f)$, we obtain a value of 89 ± 50 cm^{-1}/V for the slope of the correlation of ν_{CO} vs electrode potential. While the uncertainty is sizable, this value is clearly larger than the value, 30 cm^{-1}/V, found for CO on polycrystalline platinum surfaces.[31] However, because of the strong metal−support interaction, the surface electronic properties of the 2.5 nm sample are rather different to those of nonsupported polycrystalline samples,[6] and it is therefore reasonable to expect a difference in ν-vs-E slopes. Indeed, the experimental value found for the same sample batch but in 0.5 $HClO_4$ (as opposed to our use of H_2SO_4), was 53 ± 2 cm^{-1}/V.[18] All of these results therefore suggest that the Stark tuning effect has primarily an electronic rather than a classical electrostatic origin:[32] a more negative potential increases back-donation from Pt to the $2\pi^*$ orbital of CO, resulting in a decrease in ν_{CO}. A similar conclusiosn has been recently reached by a ^{13}C NMR study of CO adsorbed onto a polycrystalline palladium electrode.[33]

Conclusions

We have developed a phenomenological two-band model which permits a detailed analysis of the ^{13}C NMR observables of chemisorbed CO. Using this theoretical model, we have been able to obtain the partitioning of the 5σ- and $2\pi^*$-like E_f-LDOS's at ^{13}C, due to surface bonding. We find that the $2\pi^*$-like E_f-LDOS is ~10 times larger than the 5σ-like E_f-LDOS and therefore contributes significantly to the NMR observables of ^{13}C; that the change in the ^{13}C NMR observables of different samples is mainly due to the variation in the $2\pi^*$-like E_f-LDOS; and that a linear correlation appears to exist between the $2\pi^*$-like E_f-LDOS and the corresponding IR stretch frequency of adsorbed CO, indicating that changes in back-donation are responsible for the variations in chemical and physical properties of CO on platinum or platinum-based alloy surfaces. This approach is particularly useful for investigating questions relating to the activity of Pt and Pt/Ru fuel cell catalysts and their poisoning by CO which will be described in a future publication.

Acknowledgment. We are very grateful to Dr. Lamy's group in Poitiers, France, for allowing us to cite the IR data before publication, and C.R. thanks the Lamy group for their hospitality during her stay in their laboratory. Y.Y.T. thanks Dr. Y. Ben Taarit (IRC, CNRS, Villeurbanne, France) for helpful discussions. This work was supported by the United States National Science Foundation (Grant CTS 97-26419), by an equipment grant from the United States Defense Advanced Research Projects Agency (Grant DAAH 04-95-1-0581) and by the U.S. Department of Energy, Division of Materials Science, through the University of Illinois, Frederick Seitz Materials Research Laboratory (Grant DEFG02-96ER45439).

JA9922274

(27) Ewing, G. E. *J. Chem. Phys.* **1962**, *37*, 2250−2256.
(28) Tong, Y. Y.; Mériaudeau, P.; Renouprez, A. J.; Klink, J. J. v. d. *J. Phys. Chem. B* **1997**, *101*, 10155−10158.
(29) Ford, L. P.; Blowers, P.; Chen, N. C.; Lee, I. C.; Masel, R. I. *Surf. Sci.* **1999**, *419*, 144−149.
(30) Hoffmann, R. *Rev. Mod. Phys.* **1988**, *60*, 601−628.
(31) Kunimatsu, K.; Seki, H.; Golden, W. G.; II, J. G. G.; Philpott, M. R. *Surf. Sci.* **1985**, *158*, 596−608.
(32) Villegas, I.; Weaver, M. J. *J. Phys. Chem.* **1997**, *101*, 10166−10177.
(33) Vuissoz, P.-A.; Ansermet, J.-P.; Wieckowski, A. *Phy. Rev. Lett.* **1999**, *101*, 2457−2460.